Jorge Mírez
Elec. Mech, Eng.; MSc & Dr Physics
Professor
Group of Mathematical Modeling and Numerical Simulation (GMMNS)
Universidad Nacional de Ingeniería (UNI)
Lima
Perú

Jesús A. Mendoza
Professor
Universidad Nacional Experimental Politécnica Antonio José de Sucre
Bolívar
Venezuela

Simón A. Caraballo
Professor
Universidad Nacional Experimental Politécnica Antonio José de Sucre
Bolívar
Venezuela

San L. Tolentino
Research collaborator
Group of Mathematical Modeling and Numerical Simulation (GMMNS)
Universidad Nacional de Ingeniería (UNI)
Lima
Perú
Universidad Nacional Experimental Politécnica Antonio José de Sucre
Bolívar
Venezuela

Comparative Analysis of Flow Patterns in Planar and Conical Nozzles with Narrow Divergent Angles

The flow pattern in supersonic nozzles applied to the aerospace area is recurrently studied, since the geometrical profiles of the internal walls have a significant effect on the development of the flow regime. In the present work, the objective is to perform a comparative analysis of the flow patterns in planar and conical nozzles with very narrow divergent angles, for half-angle α = 1°, 1.21° and 2°. The viscous flow field was simulated in 2D with the ANSYS-Fluent R16.2 code. The RANS model and the SAS turbulence model were used for the transient state flow conditions. For viscosity as a function of temperature, the Sutherland's law equation was used. Numerical results of the flow field were obtained for the NPR range 3.98 to 6.95. In the divergent the shock train is presented, being for the conical nozzle the one with the highest velocity fluctuation in the shock fronts. For the flow at the nozzle outlet, for pressure load NPR 6.95, the conical nozzle with α = 1° has an average Mach number velocity increase of 8.81% with respect to the planar nozzle; likewise, for α = 1.21° it has an increase of 9.73% and for α = 2° it has an increase of 12.88%, respectively.

Keywords: *Comparative analysis, Conical nozzle, Flow patterns, Mach number, Planar nozzle, Shock train, Velocity fluctuations*

1. INTRODUCTION

The study of the flow field in supersonic nozzles applied to the aerospace area is recurrent. The geometries of supersonic nozzles are diverse, such as bell-shaped, parabolic, conical, planar, among other geometries [1], [2]. Nozzle sizes vary according to the thrust force required. The geometric configurations of the convergent, throat and divergent of supersonic nozzles have a significant effect on the flow development. Under the conditions of the nozzle pressure ratio (NPR), the flow in the nozzle can be underexpanded, adapted or overexpanded [1]. The set of normal, oblique and reflected waves is known as shock train, which occurs under certain pressure conditions in straight ducts, nozzles with very narrow divergent angles, supersonic nozzles with straight cut throat. As well as, in injectors, diffusers, among other mechanical devices [3,4].

Normal, oblique and reflected shock waves interact with the velocity boundary layer and thermal boundary layer in the flow regions adjacent to the nozzle walls [5-7]. In the flow field, eddies, the restricted shock separation (RSS) and free shock separation (FSS) are present [7]. The flow pressure gradients are unstable, and the lateral pressure loads act on the nozzle walls which has a temperature gradient due to the effect of flow friction [8-10]. Prandtl-Meyer expansion waves occur at the nozzle trailing edge [7]; as well as, the plume has a configuration of waves in the supersonic jet outside the nozzle.

The studies of the flow behavior in experimental nozzles in the laboratory allow recording the experimental pressure and temperature data, as well as capturing images of the shapes of the shock waves inside and outside the nozzle with the Schlieren technique [7]. And, by using computational fluid dynamics (CFD) it is possible to reproduce the turbulence of the flow, obtaining approximate solutions of thermodynamic parameters of the flow field [11].

Experiments performed by Arora and Vaidyanathan [12] for a planar nozzle with double divergence reported that the angle of inflection affects the shock structure. Verma and Manisankar [13] observed that the structure of the oblique and reflected waves presents an asymmetry, and in front of the shock front a counterflow region is present. Bourgoing and Reijasse [14] reported that the wall roughness has an effect on the flow development, they obtained different configurations of asymmetry of the shock wave structure. Mason et al. [15] addressed pressure experiments on the nozzle wall, for very narrow divergent angles, they reported that the throat curvature has a significant effect on the flow development. Weiss et al. [16] reported that the shock train, as the wave propagates its intensity decreases downstream. Tolentino and Mírez [17] reported the effect of the very narrow angle of planar-walled supersonic nozzles, which induces the formation of the shock train. Vignesh et al. [18] studied the shock train characterizations in divergent channels with planar walls for very narrow divergent angles, where the flow development is affected by the divergent walls, which induces the presence of the shock train.

Received: April 2025, Accepted: June 2025
Correspondence to: Dr. San L. Tolentino, Group of Mathematical Modeling and Numerical Simulation, Universidad Nacional de Ingeniería (UNI), Lima, Perú
E-mail: stolentino@unexpo.edu.ve
doi: 10.5937/fme2503372M

An illustrative schematic of the presence of the shock train at very narrow angles of the divergent in supersonic nozzles is shown in Fig. 1a. As well as, Fig. 1b, 1c and 1d shows the laboratory image capture of the shock train in experimental equipment with narrow divergent angles.

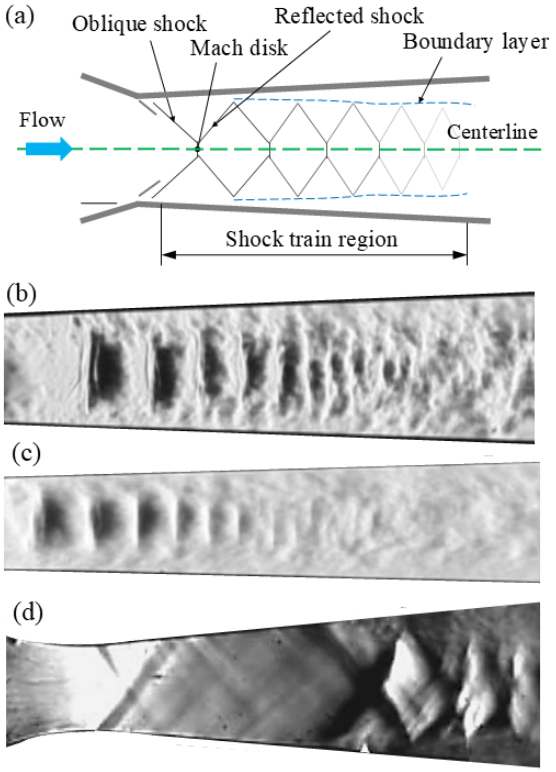

Figure 1. (a) Illustrative basic schematic of the shock train structure in the divergent for a very narrow angle nozzle [19]. (b) and (c) Shock train in a divergent duct reported by Weiss et al. [16] and, (d) reported by Matsuo et al. [4].

For the case of flow behavior in nozzles with throat length, Tolentino et al. [19] evaluated different geometric configurations of throat length in conical nozzles. Tolentino and Mírez [20] analyzed the effect of throat length on flow patterns in conical nozzles. As well as, Tolentino et al. [21] analyzed the flow behavior in planar nozzles with throat length for different divergent angles. As the throat length increases, oblique waves propagate in that section. The intensity of the flow fluctuation is most intense at the beginning of the shock train and minimal at the end, where the flow velocity is damped. The fluctuations are of greater magnitude for the conical nozzle with respect to the planar nozzle.

Other authors also conducted studies on the shock train, they are cited below: Mousavi and Roohi [22] studied the flow in a planar nozzle with very narrow angle of divergence. Roy and Ghosh [23] addressed the study of the shock train by Large-eddy simulation. Yuan et al. [24] addressed the study of flow in a supersonic duct. Zhang et al. [25] studied the asymmetric structure of the oblique shock train, for the flow in a duct. As well as, Li [26] studied the fluctuation of the shock train in a scramjet.

The interest of the study has been focused on flow patterns with the presence of shock train in nozzles with very narrow divergence angles, which are off-design nozzles. The off-design nozzles have the divergent half-angle α less than 12° [1]. From the above, was motivated to continue the research based on the work of Mason et al. [15] for a particular case of the geometry of an experimental planar nozzle classified as model A1, which has the divergent half-angle α = 1.21°, and such divergent angle is very narrow. By extending the study of the flow behavior with computational tools, approximate results of the flow field development can be obtained, as well as comparisons with supersonic conical nozzle geometries.

The objective of the present work is to analyze the flow behavior in planar and conical nozzles for divergent half-angle α = 1°, α = 1.21° and α = 2°, for which the experimental data of the planar nozzle reported by Mason et al. [15] are used. As well, Mach number and nozzle outlet pressure results are compared with isentropic flow data. Viscous flow turbulence is simulated with CFD tools, for the range of NPR 3.98 up to 6.95. Section 2 presents the methodology employed. Section 3 presents the results. Then, Section 4 presents the conclusions of the analysis performed.

2. MATERIALS AND METHODS

2.1 Experimental Nozzle

The experiment of the flow pressures in the planar nozzle (model A1) was performed at the NASA Langley Research Center 16-Foot Transonic Tunnel Complex [15]. The planar nozzle with α = 1.21° has been designed for isentropic flow: area ratio A_e/A_t = 1.09, Mach number M_d = 1.35, NPR_d = 2.97 and throat width of 10.157 cm. It should be noted; the model A1 planar nozzle has been used by Mason et al. [15] for flow pressure measurements at the nozzle walls in the range of 1.99 ≤ NPR ≤ 9.24. Where NPR = P_o/P; P_o is the total pressure at the nozzle inlet and P is the static pressure of the local atmosphere. The air flow enters the nozzle at total temperature T_o = 300 K. Being the ambient pressure and temperature of the local atmosphere P = 101.3 kPa and T = 300 K. A simple schematic of the planar nozzle (model A1) and its geometrical parameters is shown in Fig. 2, and the dimensions of the geometrical parameters are given in Table 1, Other dimensions of the geometrical parameters of the planar nozzle in question are reported in [15].

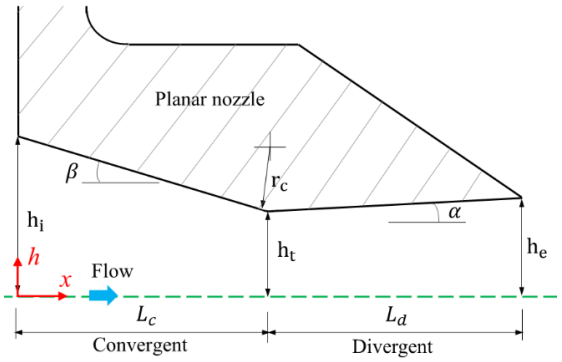

Figure 2. Basic and adapted schematic of the planar nozzle geometry (model A1) used by Mason et al. [15] for experimental compressible flow pressure tests.

In the present work, the planar nozzle (model A1) has been included as a comparative pattern for a group

of three planar nozzles, as well as, a group of three conical nozzles has been included. The half-angle of the divergent of the planar nozzles and conical nozzles are α = 1°, α = 1.21° and α = 2°. It should be noted that all geometrical dimensions projected on the 2D plane are the same for the planar and conical nozzles. The parameter h_e is a variable depending on the divergent angle. In addition, for the conical nozzle case, the parameters h_i, h_t, and h_e are the radii.

Table 1. Geometric parameters of the planar nozzle [15]. Units are in centimeters (cm).

Parameter	Value
Convergent: half-angle, β	20.84°
Divergent: half-angle, α	1.21°
Height at the nozzle inlet, h_i	3.52 cm
Nozzle throat height, h_t	1.37 cm
Radius of curvature of the throat, r_c	0.68 cm
Convergent length, L_c	5.78 cm
Divergent length, L_d	5.78 cm

2.2 Mathematical Fundamentals

For the simulation of the viscous flow field in transient state, the Reynolds-averaged Navier-Stokes (RANS) equ–ations were used with the ANSYS-Fluent R16.2 [27] code applying the finite volume method (FVM) [11]. The governing equations in transient state are the conservation of mass Eq. (1), momentum Eq. (2) and energy Eq. (3) [7,27]. Which, in compact form are expressed as:

$$\frac{\partial \rho}{\partial t} + \nabla \cdot \left(\rho u_i \right) = 0 \tag{1}$$

where, t is the time, ρ is the density and u is velocity.

$$\frac{\partial}{\partial t}\left(\rho u_i \right) + \nabla \cdot \left(\rho u_i u_j \right) = -\nabla p + \nabla \cdot \left(\overline{\overline{\tau}} \right) + \nabla \cdot \left(-\rho \overline{u_i' u_j'} \right) \tag{2}$$

where, p is the pressure and $\overline{\overline{\tau}}$ is the stress tensor. $-\rho \overline{u_i' u_j'}$ is the Reynolds stress, in which the turbulence models are coupled to close Eq. (2).

$$\frac{\partial}{\partial t}\left(\rho E \right) + \nabla \cdot \left(u_i \left(\rho E + p \right) \right) = \nabla \cdot \left(k_{eff} \nabla T + \left(\overline{\overline{\tau}}_{eff} \cdot u_i \right) \right) \tag{3}$$

where, E is the total energy, k_{eff} is the effective thermal conductivity, k_{eff} is the temperature, and $\overline{\overline{\tau}}_{eff}$ is the ef–fective stress tensor.

The SAS (Scale-Adaptive Simulation) model of Menter and Egorov [28] was used to model the turbulence of the flow field. For the flow viscosity as a function of temperature, the Sutherland's law equation was used [7] (Schlichting & Gersten, 2017). The Mach number range M is classified as: subsonic flow $0.3 \leq M$ 0.8, transonic flow $0.8 \leq M$ 1.2, supersonic flow $1.2 \leq M$ 5, hypersonic flow $M > 5$, sonic flow $M = 1$, and incompressible flow $M < 0.3$ [29].

2.3 Computational Domain

The 2D computational domain of the planar nozzle with α = 1.21° is illustrated in Fig. 3a, and it is the same computational domain that is applied for the conical nozzle, which is not included in Fig. 3 because they are similar. In total, three computational domains were constructed for the planar nozzle and three compu–tational domains for the conical nozzle, for the diver–gent half-angle α = 1°, α = 1.21° and α = 2°.

The meshing of the domain is illustrated in Fig. 3b, which includes the nozzle section and a region of the atmosphere environment. In addition, an enlarged detail of the divergent mesh is shown in Fig. 3c. The geometry of the nozzle was constructed with data reported by Mason et al. [15]. It should be noted, the 2D compu–tational domain for symmetric geometries significantly decreases the time of iterative calculations of the flow field, thus, it has a great advantage over 3D compu–tational domains.

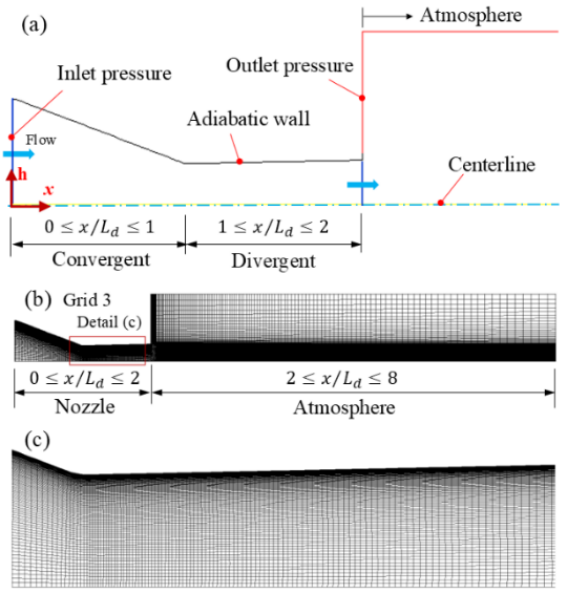

Figure 3. (a) 2D computational domain, showing the boun–dary conditions in the nozzle and in the atmosphere. (b) Grid 3 with 26385 quadrilateral cells. (c) Enlarged detail of the mesh of the divergent nozzle.

The boundary conditions applied to the 2D compu–tational domain (Fig. 3a) for the planar and conical nozzle with α = 1°, α = 1.21° and α = 2°, are as follows: Table 2 presents the pressure and temperature data at the nozzle inlet and the pressure and temperature data in the atmosphere region.

Table 2. Pressure and temperature parameters of the flow in the planar nozzle and conical nozzle.

Flow at nozzle inlet	
Total pressure:	P_o = NPR·(101300 Pa) for NPR 3.98 NPR 4.97, NPR 5.97 and NPR 6.95
Total temperature:	T_o = 300 K
Flow in the atmospheric environment	
Static pressure:	P = 101300 Pa
Static temperature:	T = 300 K

The flow is simulated for the range of NPR 3.98 to 6.95. The static pressure and temperature of the atmos–phere being P = 101.3 kPa and T = 300 K. The nozzle walls are considered adiabatic, and the flow velocity at the wall is zero because of the no-slip condition. In symmetry, the flow velocity in the axial direction of the

centerline is zero. The effect of gravity in the atmosphere region for the convective effect of the supersonic jet was not taken into account, and it is because the 2D domains of the nozzles are for symmetric geometries.

The air flow was considered as an ideal gas: gas constant R = 287 J/(kg·K), specific heat ratio k = 1.4, specific heat at constant pressure C_p = 1006.43 J/(kg·K) and thermal conductivity k_t = 0.042 W/(m·K) [27].

2.4 Numerical Convergence Analysis

The 2D computational domain of the planar nozzle with α = 1.21° was meshed in the ANSYS-Meshing platform and discretized using ICEM-CFD interaction. The mesh was refined in regions adjacent to the walls, since the flow in those regions presents shear stresses. The meshing (grid 3: 26385 cells) of the computational domain illustrated in Fig. 3b corresponds to an analysis previously performed by a numerical convergence analysis study for four grid densities, for transient state flow with the SAS turbulence model [28] for NPR 3.98.

Grids 3 and 4 presented similar results and lower magnitudes with respect to grids 1 and 2, both for wall Y-plus (y^+) (Fig. 4a) in the value of shear stress and wall shear stress (Fig. 4b).

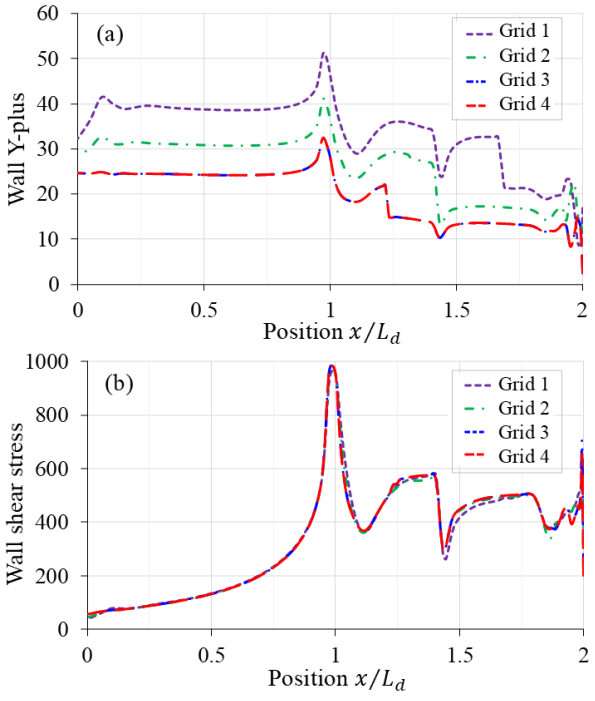

Figure 4. Values of (a) Wall Y-plus and (b) Wall shear stress for the flow at the planar nozzle wall, for NPR 3.98 and four grid densities, evaluated with the SAS turbulence model.

The average Mach number for the air flow at the nozzle outlet was also evaluated by numerical methods, and Mach 1.3509 was obtained (Table 3), where the values of grid 3 and 4 are equal. The numerical values of Mach 1.3509 were compared for isentropic flow Mach 1.35, where the percentage error for the numerical methods yielded 0.0666% (Table 3). From the above, grid 3 is taken into account to simulate the flow field, since it saves iterative calculation time with respect to grid 4, since the latter has a higher density of cells.

Table 3. Mach number (avg.) at the exit of the planar nozzle for NPR 3.98.

Grid:	1	2	3	4
Grid cells:	15184	19931	26385	29819
Mach (avg.):	1.3515	1.3516	1.3509	1.3509
Error (%):	0.1111	0.1185	0.0666	0.0666

2.5 Validation of the SAS Turbulence Model

It should be noted that turbulence models are semi-empirical transport equations that model mixing and diffusion enhanced by turbulent eddies as a function of fluid viscosity and turbulent viscosity, among other variables, which are defined by their mathematical structure consisting of a single equation or two equations [11]. It should be noted that turbulence models are evaluated on a recurring basis for both incompressible and compressible flow [30-34] in order to simulate flow turbulence and determine which turbulence model best fits the experimental data.

Three turbulence models for viscous flow in transient state for NPR 3.98 were evaluated for the grid 3 domain. The turbulence models DES SA of Spalart et al. [35], DES SST k-ω of Menter et al. [36] and SAS of Menter and Egorov [28] were compared with experimental pressure data that have been reported by Mason et al. [15]. Fig. 5 shows the curves of the three turbulence models, which are superimposed on the experimental pressure data [15] at the nozzle wall. The SAS turbulence model fits the pressure data best, which presents the smallest magnitude of the sum of the squared error Σe^2 = 0.0042277 with respect to the other turbulence models evaluated. For the DES SA model the value of Σe^2 = 0.0050792 and for the DES SST k-ω model the value of Σe^2 = 0.0042292, respectively. As well as, for the SAS model the average Mach number at the nozzle outlet was compared for the isentropic flow condition, which yielded the error of 0.0666%.

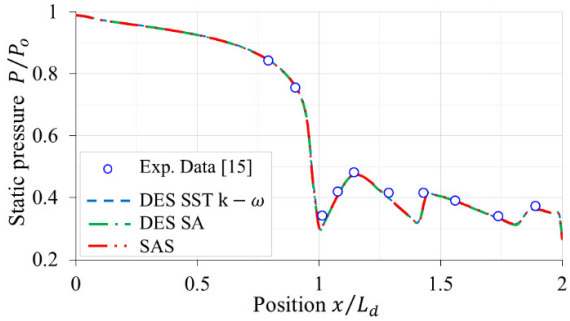

Figure 5. Comparison of three turbulence models with experimental pressure data [15] at the planar nozzle wall, for NPR 3.98 and grid 3.

2.6 Computational Solution Method

The following considerations were taken into account in the ANSYS-Fluent R16.2 code. In Solver: density-based, transient, 2D space planar (planar nozzle) and axisymmetric (conical nozzle), In solution methods; formulation: implicit, flux type: Roe-FDS, spatial discretization: least squares cell based and second order upwind, transient formulation: second order implicit. Solution initialization: hybrid. Monitor residual: $1x10^{-5}$.

To obtain the numerical solutions of the compressible flow field, the flow was simulated with the SAS turbulence model for NPR range 3.98 to 6.95, for which numerical calculations were performed in the range of 12300-42000 iterations.

3. RESULTS AND DISCUSSION

In this section, computational simulations of the flow field for the geometries of three planar nozzles and three conical nozzles for pressure loads NPR 3.98, NPR 4.97, NPR 5.97 and NPR 6.95 are presented. In the flow field of Fig. 6, Fig. 7 and Fig. 8, the red colored regions represent higher magnitude values and the blue colored regions represent lower magnitude values.

3.1 Mach Number

The Mach number flow field for the planar and conical nozzles is illustrated in Fig. 6 for the nozzle with $\alpha = 1°$, Fig. 7 for the nozzle with $\alpha = 1.21°$ and Fig. 8 for the nozzle with $\alpha = 2°$. The profiles evaluated at the cen–terline are shown in Fig. 9, Fig. 10 and Fig. 11. It is observed for the planar nozzle and conical nozzle that there is a large difference in the behavior of the flow patterns in the divergent ($1 \leq x/L_d \leq 2$) and in the atmosphere region ($2 \leq x/L_d \leq 8$) for each NPR value. Whereas, in the convergent ($0 \leq x/L_d \leq 1$) the flow pat–terns are similar. In the divergent of the nozzles the shock train conformed by oblique and reflected waves are presented, and the flow discharged in the region of the atmosphere presents velocity oscillations.

The flow in the planar and conical nozzle (Fig. 6, Fig. 7, Fig. 8, Fig. 9, Fig. 10 and Fig. 11) for the values of NPR 3.98, NPR 4.97, NPR 5.97 and NPR 6.95 the flow is fully developed. In the divergent, in the region of the shock train, the flow is accelerated and decce–lerated which produces the shock fronts. The intensity of the flow fluctuations of the planar nozzle is lower with respect to the conical nozzle.

For the case of the planar nozzle for the range of NPR 3.98 to NPR 6.95 (Fig. 9a, Fig. 10a, Fig. 11a and Table 4), in the divergent section ($1 \leq x/L_d \leq 2$), the nozzle with $\alpha = 1°$ presents the first shock front, which the flow accelerates to the maximum velocity Mach 1.398 at position $x/L_d = 1.214$, then the flow decelerates to the minimum velocity Mach 1.124 at position $x/L_d = 1.255$. The second shock front presents the maximum velocity Mach 1.352 at position $x/L_d = 1.57$ and mini–mum velocity Mach 1.219 at position $x/L_d = 1.632$. For a slight increase of the divergent half-agle, for $\alpha = 1.21°$ and $\alpha = 2°$, the positions of the shock fronts are slightly shifted towards the nozzle exit, as well as, the magnitude of the maximum and minimum Mach number velocity is increased.

Regarding the comparison of the maximum flow velocity in the divergent of the planar nozzle with $\alpha = 1°$, for the nozzle with $\alpha = 1.21°$ the first shock front reaches Mach 1.41 with an increase of 0.85%; the second shock front reaches Mach 1.382 with an increase of 2.21%. As well as, for the nozzle with $\alpha = 2°$ the first shock front reaches Mach 1.462 with an increase of 4.57%; the second shock front reaches Mach 1.495 with an increase of 10.57%.

The flow at the throat at position $x/L_d = 1$ has Mach 0.849 and are the same values for the nozzle with $\alpha = 1°$, $\alpha = 1.21°$ and $\alpha = 2°$, the reason for the same nume–rical magnitude is because the flow is choked. At the exit of the nozzle at position $x/L_d = 2$, the nozzle with $\alpha = 1°$ reaches Mach 1.36, for $\alpha = 1.21°$ it reaches Mach 1.407 and for $\alpha = 2°$ it reaches Mach1.45, being for the latter a velocity increase of 6.61%.

While, for the case of the conical nozzle for $\alpha = 1°$ $\alpha = 1.21°$ and $\alpha = 2°$ and for the range of NPR 3.98 to NPR 6.95 (Fig. 9b, Fig.10 b, Fig. 11b and Table 4), in the divergent section ($1 \leq x/L_d \leq 2$) a different behavior is presented than for the planar nozzle, with shifts of the positions of the shock fronts and increases of the Mach number magnitude when the half-angle of the divergent is increased.

The conical nozzle with $\alpha = 1°$ presents the first shock front, the flow accelerates to the maximum velo–city Mach 1.541 at position $x/L_d = 1.206$, then the flow decelerates to the minimum velocity Mach 0.926 at position $x/L_d = 1.239$. The second shock front has the maximum velocity Mach 1.427 at position $x/L_d = 1.546$ and minimum velocity Mach 1.183 at position $x/L_d = 1.607$.

Regarding the comparison of the maximum flow velocity at the divergent of the conical nozzle with $\alpha = 1°$, for the nozzle with $\alpha = 1.21°$ the first shock front reaches Mach 1.564 with an increase of 1.49%; the second shock front reaches Mach 1.473 with an increase of 3.22%. As well as, for the nozzle with $\alpha = 2°$ the first shock front reaches Mach 1.668 with an increase of 8.24%; the second shock front reaches Mach 1.656 with an increase of 16.04%.

At position $x/L_d = 1$, which corresponds to the throat section, the flow presents the same Mach number value 0.81 for the nozzle with $\alpha = 1°$, $\alpha = 1.21°$ and $\alpha = 2°$. At the nozzle outlet at position $x/L_d = 2$, for the nozzle with $\alpha = 1°$ the flow reaches Mach 1.386, for the nozzle with $\alpha = 1.21°$ it reaches Mach 1.524 and for the nozzle with $\alpha = 2°$ it reaches Mach 1.629, being for the latter a velocity increase of 21.13%.

The values obtained for the positions of the shock front in the divergent show that, for the case of the conical nozzle, the position of the shock front presents a smaller stroke with respect to the planar nozzle, as well as the shock train in the conical nozzle presents a higher intensity of jump of the flow fluctuation.

At the position $x/L_d = 1$ of the centerlines for the nozzles with $\alpha = 1°$, $\alpha = 1.21°$ and $\alpha = 2°$ (Fig. 9, Fig. 10, Fig. 11 and Table 4), the flow velocity of the conical nozzle decreases by 4.59% with respect to the planar nozzle. As well as, at the $x/L_d = 2$ position of the conical nozzle, the flow velocity for the nozzle with $\alpha = 1°$ has an increase of 1.91%, for the nozzle with $\alpha = 1.21°$ has an increase of 8.31% and for the nozzle with $\alpha = 2°$ has an increase of 15.79%, respectively.

For the flow expanding in the region of the atmosphere (Fig. 9, Fig. 10 and Fig. 11), the conical nozzle exhibits higher velocity jump and higher flow velocity fluctuation with respect to the planar nozzle. For both nozzle geometries, the intensity of the

fluctuation decreases slightly with increasing divergent angle. For the case of the planar nozzle with α = 1° and NPR 6.95, the highest peak maximum velocity is Mach 2.64 at position x/L_d = 2.92; while from the conical nozzle it is Mach 3.5 at position x/L_d = 2.837, which has a velocity increase of 32.57%. For the planar nozzle with α = 2°, the highest peak maximum velocity reaches Mach 2.55 at position x/L_d = 2.97; while that of the conical nozzle is Mach 3.05 at position x/L_d = 2.73, which has a velocity increase of 37.25%.

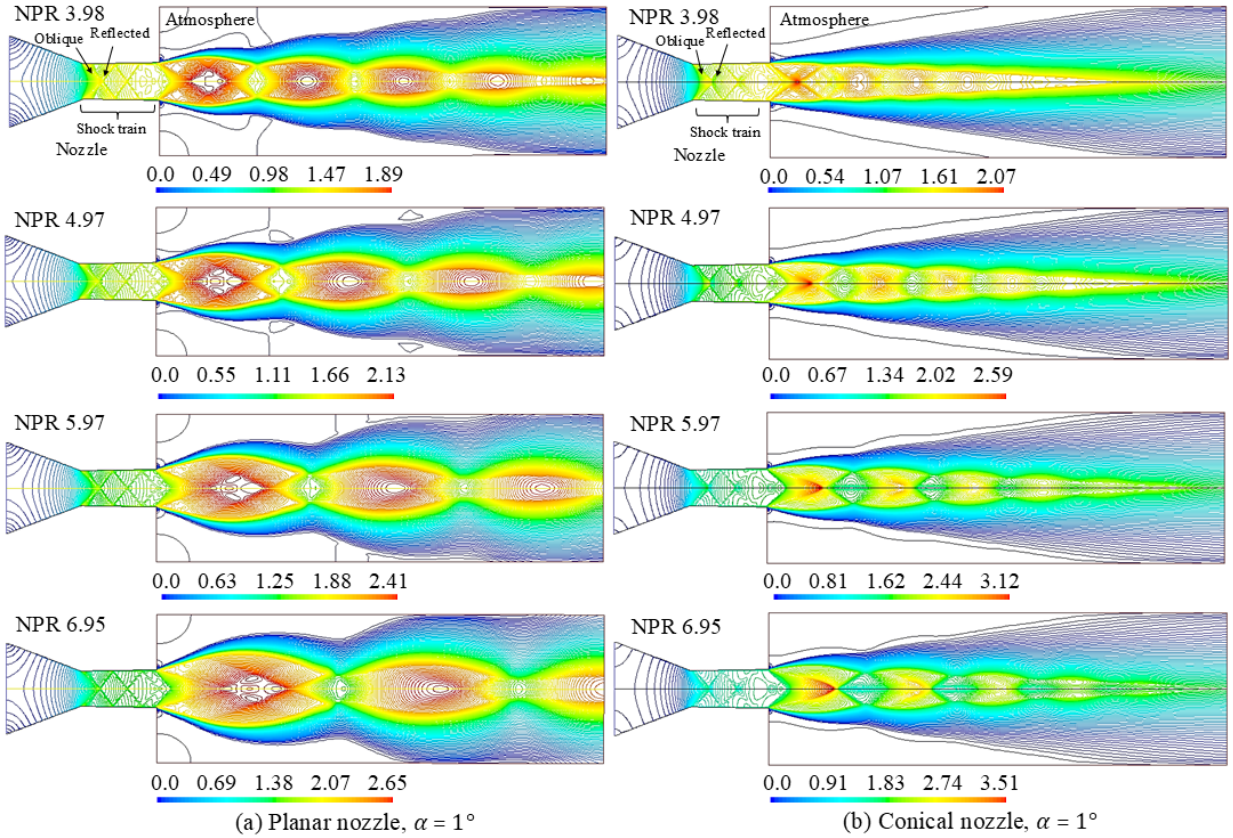

Figure 6. Mach number flow field for the divergent with α = 1°: (a) Planar nozzle and (b) Conical nozzle.

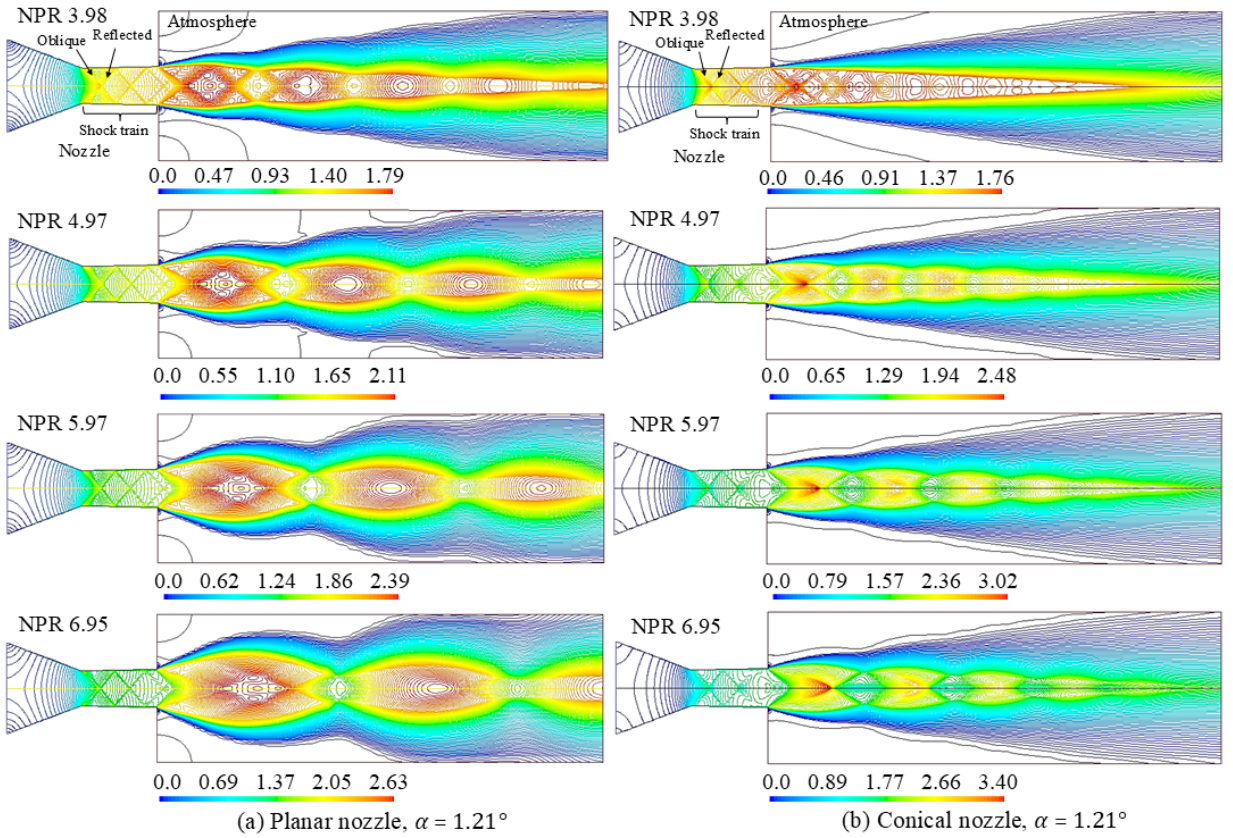

Figure 7. Mach number flow field for the divergent with α = 1.21°: (a) Planar nozzle and (b) Conical nozzle.

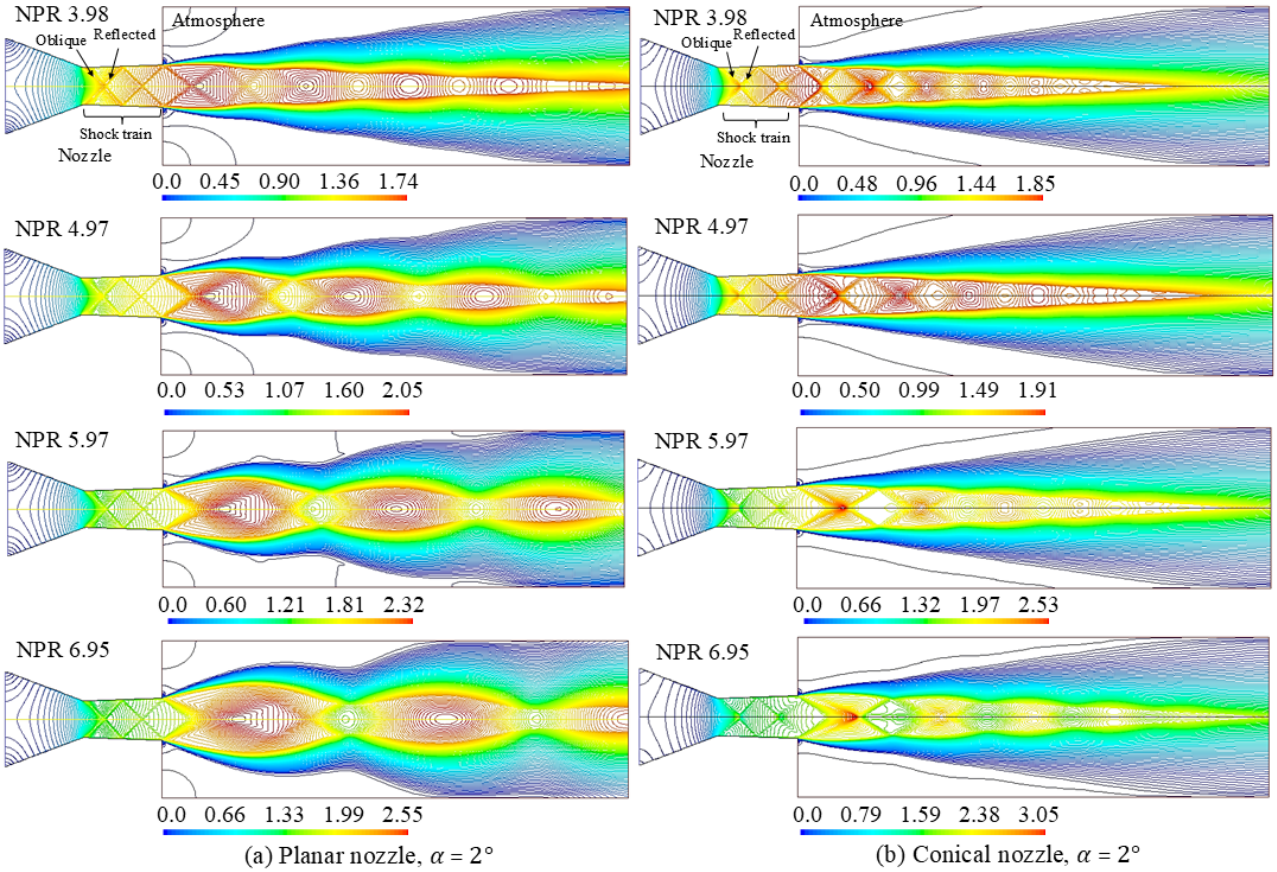

Figure 8. Mach number flow field for the divergent with α = 2°: (a) Planar nozzle and (b) Conical nozzle.

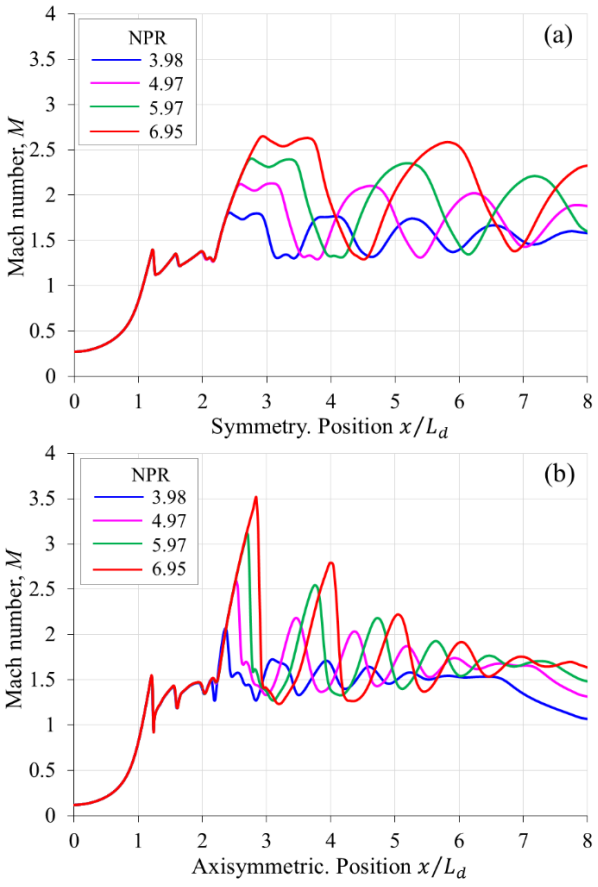

Figure 9. Mach number profiles on the centerline for the divergent with α = 1°: (a) Planar nozzle and (b) Conical nozzle.

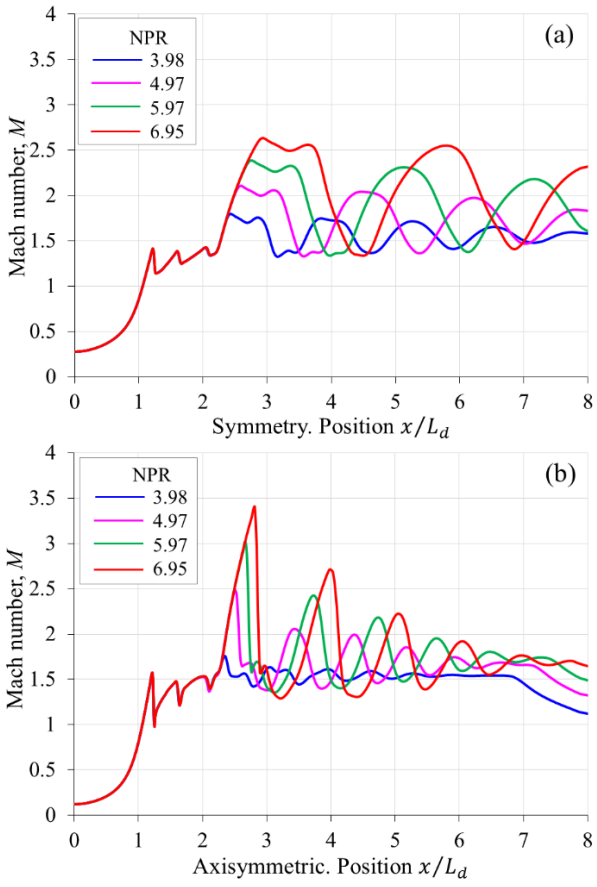

Figure 10. Mach number profiles on the centerline for the divergent with α = 1.21°: (a) Planar nozzle and (b) Conical nozzle.

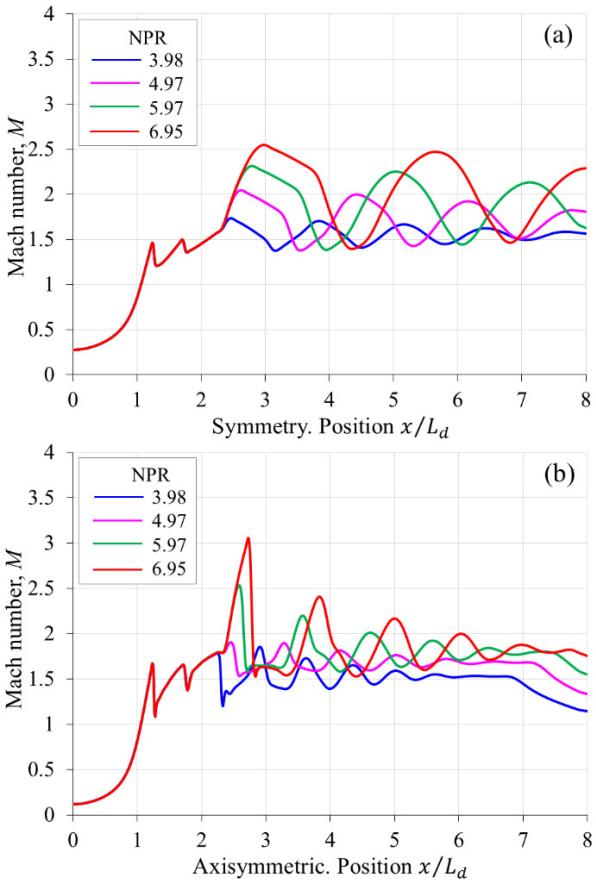

Figure 11. Mach number profiles on the centerline for the divergent with α = 2°: (a) Planar nozzle and (b) Conical nozzle.

Table 4. Velocity fluctuations in the region of the shock train evaluated at the divergent centerline ($1 \le x/L_d \le 2$) for NPR NPR 3.98, NPR 4.97, NPR 5.97 and NPR 6.95.

Planar nozzle		Conical nozzle	
Position x/L_d	Mach number	Position x/L_d	Mach number
Divergent: α = 1°			
1	0.849	1	0.810
1.214	1.398	1.206	1.541
1.255	1.124	1.239	0.926
1.570	1.352	1.546	1.427
1.632	1.219	1.607	1.183
2	1.360	2	1.386
Divergent: α = 1.21°			
1	0.849	1	0.810
1.217	1.410	1.209	1.564
1.266	1.138	1.241	1.006
1.601	1.382	1.577	1.473
1.663	1.246	1.638	1.210
2	1.407	2	1.524
Divergent: α = 2°			
1	0.849	1	0.810
1.239	1.462	1.239	1.668
1.317	1.208	1.281	1.094
1.697	1.495	1.711	1.656
1.781	1.356	1.781	1.378
2	1.450	2	1.679

The average Mach number for viscous flow was evaluated by numerical integration at the outlet of the planar nozzle and the conical nozzle in perpendicular direction of the symmetry axis towards the wall at the position $x/L_d = 2$, whose results are presented in Table 5.

It should be noted that the average values of the Mach number are slightly different for the same value of the half-angle of the divergent and this is due to the iterative results of the numerical calculations of approximate solutions generated by the same CFD software. However, the first two decimal digits have satisfactory correspondence as an approximate solution.

It is observed that the Mach number (avg.) increases as the divergent angle increases, and the magnitude is higher for the case of the conical nozzle. Taking as reference for NPR 6.95, the conical nozzle with α = 1° increases its velocity 8.81% with respect to the planar nozzle with α = 1°. Next, for α = 1.21° it increases its velocity 9.73% with respect to the planar nozzle with α = 1.21°. Likewise, for the conical nozzle with α = 2° it increases its velocity 12.88%. However, as the exit area of the conical nozzle is smaller than that of the planar nozzle, the mass flow varies, therefore, the thrust force in both nozzles is different, being lower for the conical nozzle.

Table 5. Average Mach number at the exit of the planar nozzle and conical nozzle.

NPR:	3.98	4.97	5.97	6.95
Divergent:	Planar nozzle: Mach number (avg.)			
$\alpha = 1°$	1.325	1.326	1.327	1.328
$\alpha = 1.21°$	1.350	1.353	1.355	1.356
$\alpha = 2°$	1.452	1.456	1.457	1.459
Divergent:	Conical nozzle: Mach number (avg.)			
$\alpha = 1°$	1.428	1.440	1.441	1.445
$\alpha = 1.21°$	1.475	1.482	1.486	1.488
$\alpha = 2°$	1.626	1.640	1.644	1.647

The numerical results of the 2D simulations for viscous flow of the average Mach number (Table 5) at the outlet of the planar nozzle and conical nozzle for α = 1°, α = 1.21° and α = 2° and for the pressure loadings NPR 3.98, NPR 4.97, NPR 5.97 and NPR 6.95, are compared with respect to isentropic flow, and the comparison curves are shown in Fig. 12. In addition, the relative percentage errors of the Mach number comparison are shown in Fig. 13. It should be noted, the design conditions for adapted and isentropic flow of the planar nozzle for α = 1° is Mach 1.317, for α = 1.21° is Mach 1.35 and for α = 2° is Mach 1.455. Likewise, for the conical nozzle for α = 1° is Mach 1.464, for α = 1.21° is Mach 1.514; on the other hand, for the case with α = 2° the adapted flow is Mach 1.676 for NPR ≥ 4.76, therefore, for NPR 3.98 is Mach 1.464.

For the divergent with α = 1° (Fig. 12a), the Mach number (avg.) of the planar nozzle has the highest error of 0.89% (Fig. 13), while the Mach number (avg.) of the conical nozzle has the highest error of 2.43%.

For a slight increase of the divergent angle of the planar nozzle and conical nozzle for α = 1.21° (Fig. 12b), the Mach number (avg.) of the planar nozzle has the highest error of 0.46% (Fig. 13), whereas, the conical nozzle has the highest error of 2.55%.

Likewise, for the nozzle with α = 2° (Fig. 12c), the Mach number (avg.) of the planar nozzle has the highest error of 0.27% (Fig. 13), while, the Mach number (avg.) of the conical nozzle has the highest error of 2.13%, for NPR ≥ 4.97. Based on the numerical comparison for NPR 3.98 we have for the Mach number (avg.) an error of 11%.

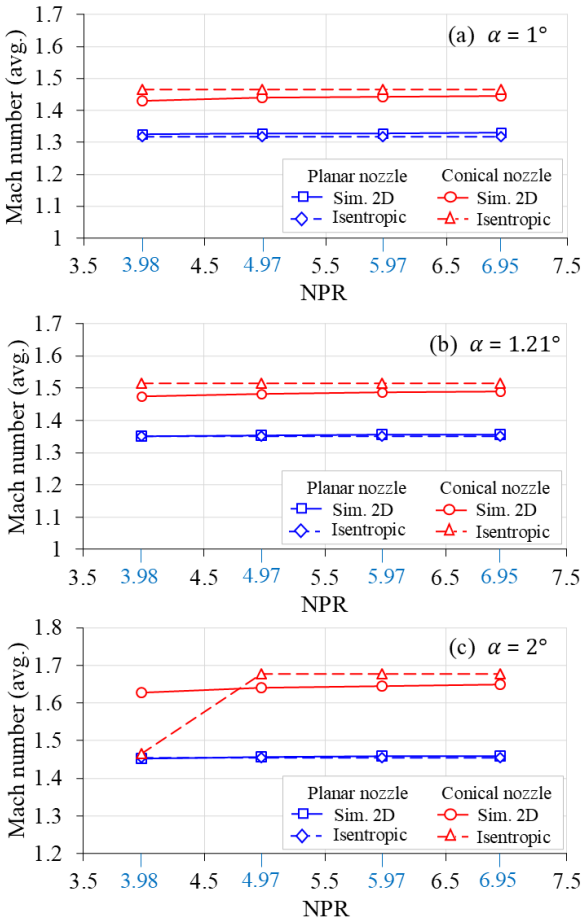

Figure 12. Comparison of average Mach number for viscous flow with respect to Mach number for isentropic flow, for the flow at the nozzle exit.

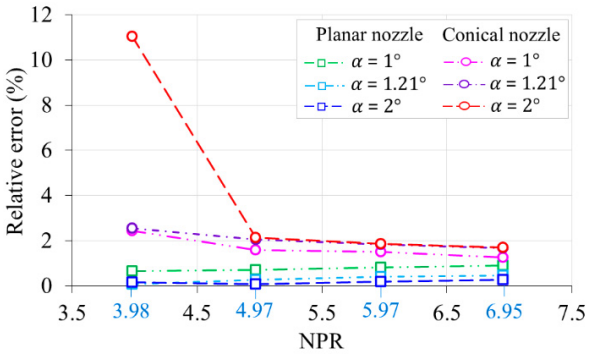

Figure 13. Percentage relative error of the average Mach number at the nozzle exit.

The numerical results of the divergent velocity fluctuations of the present work have different configurations with respect to the flow in the nozzles with straight-cut throat. Such is the case of planar nozzles with α = 11.01° [21], in the straight-cut throat the velocity fluctuations are in the range of Mach 1 to 1.2, and the centerline of the divergent, they are in the range of Mach 0.849 to 1.45 (Table 4). For the case of conical nozzles with α = 10° [19], in the straight-cut throat the velocity fluctuations are in the range of Mach 0.6 to 1.8, and in the centerline of the divergent, they are in the range of Mach 0.81 to 1.679 (Table 4). Similar results of flow patterns with presence of shock train in the divergent of the planar nozzle shown in Fig. 7a and Fig. 10a have been reported in [17] for the planar nozzle with $\alpha = 1.21°$, in which they present the shapes of the shock waveform structures in the Mach number and static pressure flow field. Therefore, the Mach number range variations in the flow region where the shock train occurs are affected by the geometrical configurations of the nozzle walls.

3.2 Static Pressure

The profiles of the static pressures evaluated in the centerline of the planar nozzle and conical nozzle are shown in Fig. 14, Fig. 15 and Fig. 16. They are related to the Mach number flow field previously presented in Fig. 6, Fig. 7 and Fig. 8.

As the divergent angle of the planar nozzle and conical nozzle increases, in the region where the shock fronts for the maximum and minimum flow velocity occur, the pressures decrease, being of lower magnitude for the conical nozzle. The numerical values of the pressure drops and positions for the first and second shock front for the nozzle with α = 1°, α = 1.21° and α = 2° are presented in Table 6. At the position $x/L_d = 1$ of the centerlines for the planar nozzles and conical nozzles with α = 1°, α = 1.21° and α = 2° (Fig. 14, Fig. 15 and Fig. 16 and Table 6), the flow pressure drop of the conical nozzle has an increase of 4% with respect to the planar nozzle. As well as, at the $x/L_d = 2$ position of the conical nozzle, the flow pressure drops for the nozzle with α = 1° decreases 6.34%, for the nozzle with α = 1.21° decreases 16.45% and for the nozzle with α = 2° decreases 29.45%, respectively.

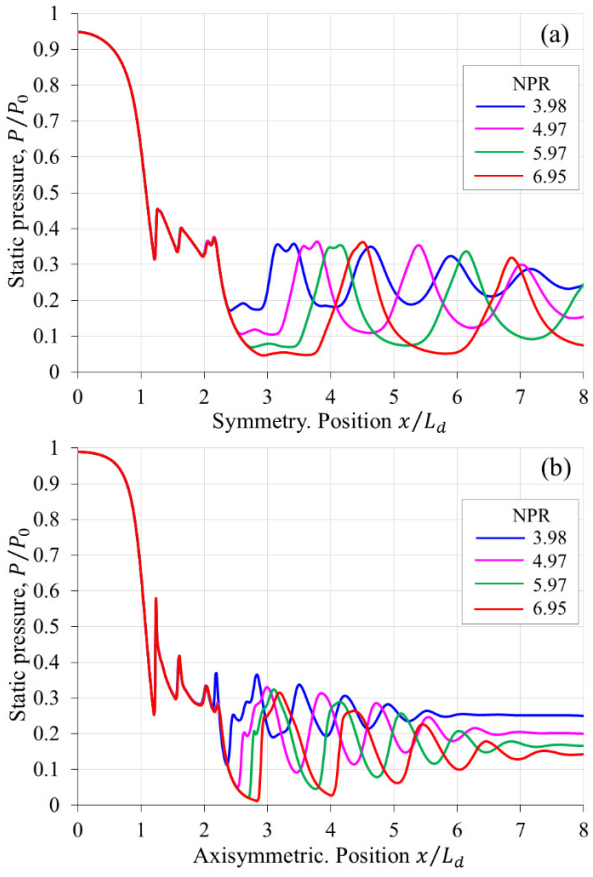

Figure 14. Static pressure profiles on the centerline for the divergent with α = 1°: (a) Planar nozzle and (b) Conical nozzle.

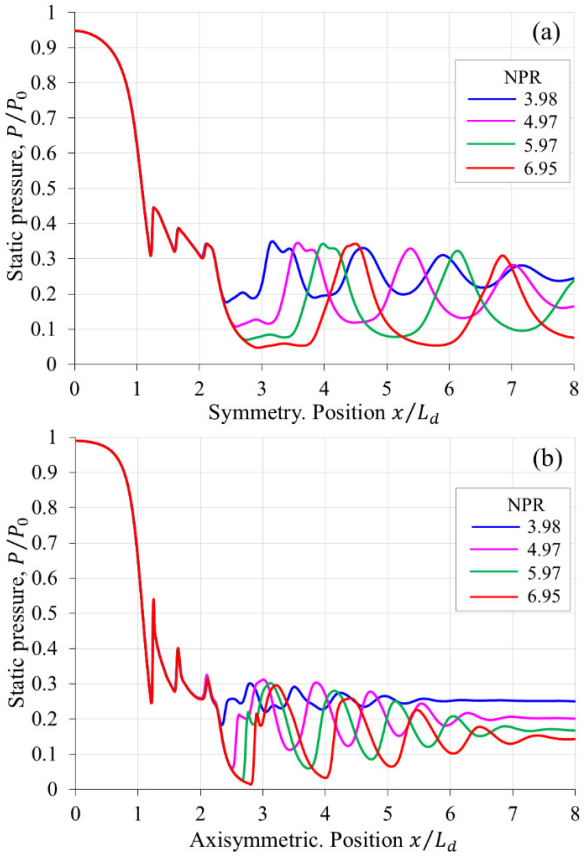

Figure 15. Static pressure profiles on the centerline for the divergent with α = 1.21°: (a) Planar nozzle and (b) Conical nozzle.

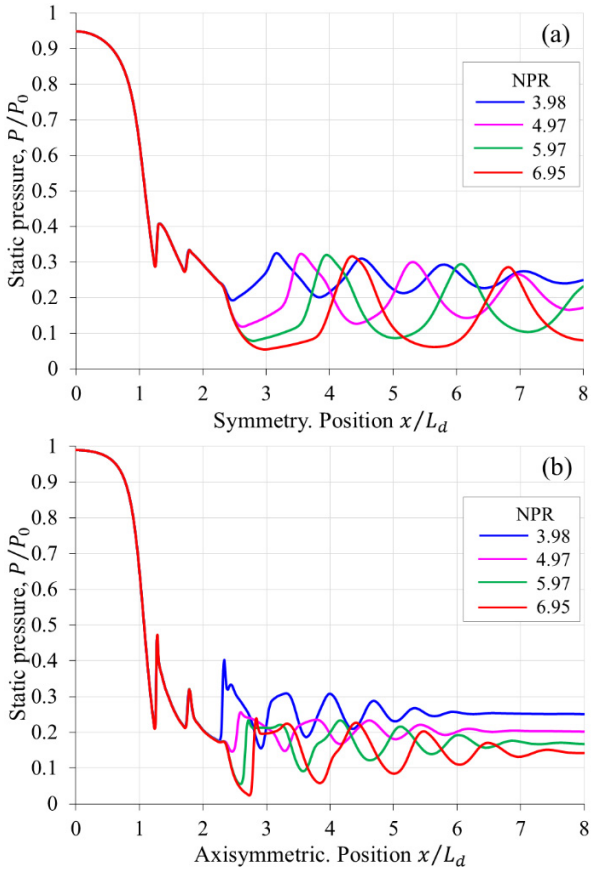

Figure 16. Static pressure profiles on the centerline for the divergent with α = 2°: (a) Planar nozzle and (b) Conical nozzle.

Table 6. Pressure fluctuations in the region of the shock train evaluated at the divergent centerline ($1 \le x/L_d \le 2$) for NPR 3.98, 4.97, 5.97 and 6.95.

Planar nozzle		Conical nozzle	
Position x/L_d	Static pressure	Position x/L_d	Static pressure
Divergent: α = 1°			
1	0.624	1	0.649
1.214	0.315	1.206	0.256
1.255	0.453	1.239	0.575
1.570	0.335	1.546	0.299
1.632	0.401	1.607	0.417
2	0.331	2	0.310
Divergent: α = 1.21°			
1	0.624	1	0.649
1.217	0.309	1.209	0.246
1.266	0.446	1.241	0.519
1.601	0.321	1.577	0.279
1.663	0.387	1.638	0.401
2	0.310	2	0.259
Divergent: α = 2°			
1	0.624	1	0.649
1.239	0.287	1.239	0.212
1.317	0.407	1.281	0.467
1.697	0.274	1.711	0.214
1.781	0.333	1.781	0.320
2	0.292	2	0.206

For flow in the region of the atmosphere, the conical nozzle exhibits lower pressure drop and higher flow fluctuation with respect to the planar nozzle. For both nozzle geometries, the fluctuation intensity decreases slightly when the divergent angle increases.

For the case of the planar nozzle with α = 1° and NPR 6.95, the lowest pressure drop is P/P_o = 0.046 at position x/L_d = 2.92; while that of the conical nozzle is P/P_o = 0.012 at position x/L_d = 2.837, which has a pressure decrease of 73.9%. For the planar nozzle with α = 2°, the lowest pressure drop is P/P_o = 0.053 at position x/L_d = 2.97; while that of the conical nozzle is P/P_o = 0.024 at position x/L_d = 2.73, which has a pressure decrease of 54.7%.

The average static pressure at the outlet of the planar nozzle and conical nozzle, at the x/L_d = 2 position, are presented in Table 7 and the data are compared with respect to the data for isentropic flow, as shown in Fig. 17. Also, the relative percentage errors of the static pressure comparison are shown in Fig. 18. It should be noted, for the pressure case, the design conditions for adapted and isentropic flow of the planar nozzle for α = 1° is P/P_o = 0.352, for α = 1.21° is P/P_o = 0.337, for α = 2° is P/P_o = 0.290. Likewise, for the conical nozzle for α = 1° is P/P_o = 0.286, for α = 1.21° is P/P_o = 0.266. As well as, for α = 2° one has P/P_o = 0.209, for NPR ≥ 4.76, therefore, for NPR 3.98 one has P/P_o = 0.251.

For the nozzle with α = 1° (Fig. 17a), the static pressure (avg.) of the planar nozzle has the highest error of 2.88% (Fig. 18), while the static pressure (avg.) of the conical nozzle has the highest error of 1.96%. For a slight increase of the divergent angle of the planar nozzle and conical nozzle for α = 1.21° (Fig. 17b), the static pressure (avg.) of the planar nozzle has the highest error of 2.41% (Fig. 18), whereas, the conical nozzle has the highest error of 1.47%.

Likewise, for the divergent with α = 2° (Fig. 17c), the static pressure (avg.) of the planar nozzle has the highest error of 2.37% (Fig. 18), while, the static pressure (avg.) of the conical nozzle has the highest error of 0.74%, for NPR ≥ 4.97. For NPR 3.98, the static pressure (avg.) has an error of 14.7%.

Table 7. Average static pressure at the exit of the planar nozzle and conical nozzle.

NPR:	3.98	4.97	5.97	6.95
Divergent:	Planar nozzle: Static pressure (avg.)			
$\alpha = 1°$	0.343	0.343	0.342	0.342
$\alpha = 1.21°$	0.330	0.329	0.329	0.328
$\alpha = 2°$	0.285	0.284	0.283	0.283
Divergent:	Conical nozzle: Static pressure (avg.)			
$\alpha = 1°$	0.292	0.286	0.286	0.285
$\alpha = 1.21°$	0.270	0.268	0.268	0.267
$\alpha = 2°$	0.214	0.211	0.210	0.210

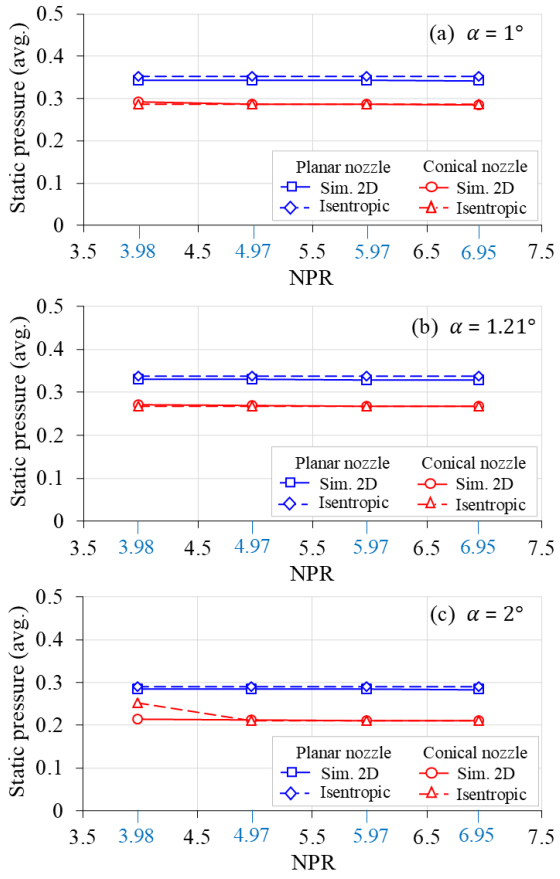

Figure 17. Comparison of average pressure for viscous flow with respect to pressure for isentropic flow, for the flow at the nozzle exit.

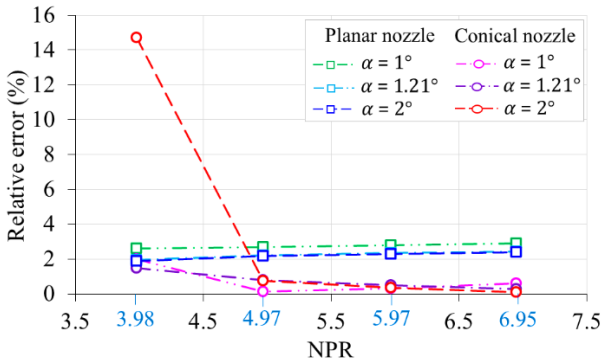

Figure 18. Percentage relative error of the average static pressure at the nozzle exit.

The pressure side loads from the computational simulations on the planar nozzle and conical nozzle are illustrated in Fig. 19, which are compared with the experimental pressure data for planar nozzle reported by Mason et al. [15].

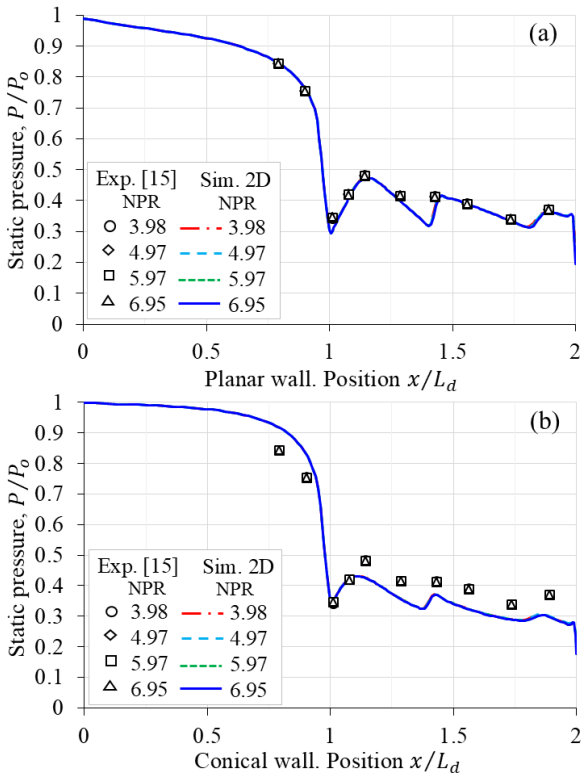

Figure 19. Comparison of pressure curve trajectories with experimental data from Mason et al. [15]. (a) Pressure on the planar nozzle wall. (b) Pressure on the conical nozzle wall.

For the case of the planar nozzle con α = 1.21° (Fig. 19a), the pressure curves of the computational simu–lations follow the trajectory of the experimental data, for NPR 3.98, NPR 4.97, NPR 5.95 and NPR 6.95. The pressure fluctuations in the divergent wall are caused by the presence of oblique and reflected waves in the shock train region, therefore, there is compression and decom–pression of the flow region adjacent to the divergent wall. The presence of the shock train is a consequence of the effect of the divergent angle, since it is very narrow, which has α = 1.21°. For the case of ducts with parallel walls, the flow behavior would be almost similar with respect to the nozzle studied in this work. However, when the divergent angle increases, the pressure fluctuations on the wall decrease since the oblique and reflected waves are with lower intensity, the flow regime has a better development, such is the case of flow study performed for the same geometry of the planar nozzle with α = 10.85° that was reported in [15, 17]. It should be noted that, a study of the cell density in the mesh for the planar nozzle with α = 1.21° was reported in [11], where the curves of the numerical pressure solutions fluctuate at the wall and which were compared with the experimental data of Mason et al. [15].

For the case of the conical nozzle con α = 1.21° (Fig. 19b), the experimental pressure data [15], which are the same as those used previously, were taken as a compa–rative standard. In the divergent one, the fluctuations of

the lateral pressure load of the computational simu–lations are smaller with respect to the planar nozzle. It is evident that the divergent geometry of the nozzle has a significant effect on the behavior of the flow patterns, therefore, the gradients of the thermodynamic para–meters, such as pressure, velocity, temperature, density, among others, are significantly affected. Therefore, the–se variations in the magnitudes of thermodynamic para–meters affect the performance of supersonic nozzles.

4. CONCLUSION

Based on the results of numerical simulations for vis–cous flow in planar nozzles and conical nozzles with half-angle $\alpha = 1°$, $\alpha = 1.21°$ and $\alpha = 2°$, the following is concluded:

The behavior of the trajectories of the Mach number and pressure pattern curves are different from each other in the divergent of both supersonic nozzles. In this sense, the geometry of the nozzle walls significantly affects the development of the flow regime, generating the shock train formed by oblique and reflected waves. The flow velocity at the outlet of the planar nozzle and the conical nozzle increases as the divergent angle increases, and the magnitude of the flow velocity with respect to Mach number (avg.) is higher for the case of the conical nozzle.

The velocity fluctuations in the regions where the divergent shock fronts occur are of greater intensity for the flow in the conical nozzle. The maximum velocity peaks at the onset of the shock fronts in the divergent section of the nozzle for the flow in the planar nozzle are in the range of Mach number 1.352 to 1.495, and for the conical nozzle in the range of Mach number 1.427 to 1.668.

For the flow at the nozzle exit with pressure load NPR 6.95, the conical nozzle with $\alpha = 1°$ has an increase in Mach number velocity (avg.) of 8.81% with respect to the planar nozzle. Likewise, for $\alpha = 1.21°$ it has an increase of 9.73% and for $\alpha = 2°$ it has an increase of 12.88%.

The Mach numbers (avg.) at the nozzle exit for viscous flow present deviations of numerical values with respect to isentropic flow. For the NPR 6.95 flow pressure load, we have the following: for the planar nozzle with $\alpha = 1°$, the Mach number (avg.) presents the error of 0.89%, while for the conical nozzle the error of 2.43% is presented. For the divergent with $\alpha = 1.21°$ the Mach number (avg.) of the planar nozzle presents the error of 0.46%, while for the conical nozzle presents the error of 2.55%. Finally, for the divergent with $\alpha = 2°$, the Mach number (avg.) of the planar nozzle presents the error of 0.27%, while, the Mach number (avg.) of the conical nozzle presents the error of 2.13%.

REFERENCES

[1] Sutton, G.P. and Biblarz, O.: *Rocket propulsion elements.* 9 ed., John Wiley and Sons: New York, 2016.

[2] Scarlatella, G. Tajmar, M. and Bach, C: Advanced nozzle concepts in retro-propulsion applications for reusable launch vehicle recovery: a case study, in: *72nd International Astronautical Congress (IAC),* Dubai, United Arab Emirates, 25-29 October, 2021, pp. 1-26. https://iafastro.directory/iac/paper/id/65514/summary/

[3] Carroll B.F., Dutton, J.C: Characteristics of mul–tiple shock wave/turbulent boundary-layer interac–tions in rectangular ducts, *Journal of Propulsion and Power*, Vol. 6, No. 2, pp. 186-193, 1990, https://doi.org/10.2514/3.23243.

[4] Matsuo, S., Kanesaki, K., Nagao, J., Khan, M., Setoguchi, T., Kim, H. D.: Effects of supersonic nozzle geometry on characteristics of shock wave structure, Open Journal of Fluid Dynamics, Vol 2, No. 2A, pp. 181-186, 2012, http://dx.doi.org/10.4236/ojfd.2012.24A019

[5] Bulat, P.V., Uskov, V.N.: Mach reflection of a shock wave from the symmetry axis of the super–sonic nonisobaric jet, *Research Journal of Applied Sciences, Engineering and Technology*, Vol. 8, No. 1, pp. 135–142. https://doi.org/10.19026/rjaset.8.951

[6] Hadjadj, A. Ben-Nasr, O., Shadloo, M.S., Chaud–huri, A.: Effect of wall temperature in supersonic turbulent boundary layers: A numerical study, *International Journal of Heat and Mass Transfer,* Vol. 81, pp. 426-438, 2015, https://doi.org/10.1016/j.ijheatmasstransfer.2014.10.025

[7] Schlichting, H. and Gersten, K.: *Boundary-layer theory*, 9 ed., Berlin Heidelberg, Germany, Springer Verlag, 2017.

[8] Zmijanović, V. Rašuo, B., Chpoun, A.: Flow sepa–ration modes and side phenomena in an overex–panded nozzle, *FME Transactions*, Vol. 40, No. 3, pp. 111-118, 2012. https://www.mas.bg.ac.rs/_media/istrazivanje/fme/vol40/3/03_vzmijanovic.pdf

[9] Fisher, C., Olivier, H.: Experimental investigation of wall and total temperature influence on a shock train, *AIAA journal*, Vol. 52, No. 4, pp. 757-766, 2014, https://doi.org/10.2514/1.J052599

[10] Génin, C. Stark, R. and Karl, S.: Shock system deformation in high Mach number rocket nozzles, in: *Sasoh A., Aotki T., Katayama M. (eds) 31st International Symposium on Shock Waves 2, ISSW 2017.* Springer, Cham., 2019, pp. 543-549, https://doi.org/10.1007/978-3-319-91017-8_69

[11] Ferziger, J.H., Perić, M., Street, R.L.: *Compu–tational Methods for Fluid Dynamics*, 4 ed., Springer, 2020.

[12] Arora, R., Vaidyanathan, A. Experimental investi–gation of flow through planar double divergent nozzles, *Acta Astronautica*, Vol. 112, pp. 200-2016, 2015, https://doi.org/10.1016/j.actaastro.2015.03.020.

[13] Verma, S.B., Manisankar, C.: Origin of flow asym–metry in planar nozzles with separation, *Shock Waves*, Vol. 24, No. 2, pp. 191–209, 2014. https://doi.org/10.1007/s00193-013-0492-1

[14] Bourgoing, A., Reijasse, P.: Experimental analysis of unsteady separated flows in a supersonic planar

nozzle, *Shock Waves,* Vol. 14, No. 4, 251–258, 2005. https://doi.org/10.1007/s00193-005-0269-2

[15] Mason, M.L., Putnam, L.E., Re, R.J.: The effect of throat contouring on two-dimensional converging-diverging nozzles at static conditions, *NASA Technical Paper 1704,* pp. 1-67, 1980. https://ntrs.nasa.gov/api/citations/19800020749/downloads/19800020749.pdf

[16] Weiss, A., Grzona, A., Olivier, H.: Behavior of shock trains in a diverging duct, *Experiments in Fluids*, Vol. 49, No. 2, pp. 355-365, 2010. https://doi.org/10.1007/s00348-009-0764-9

[17] Tolentino, S.L. and Mírez, J.: Effect of divergence on the compressible flow patterns in off-design planar nozzles, *FME transactions*, Vol. 53, No. 1, pp. 144-156, 2025. https://doi.org/10.5937/fme2501144T

[18] Vignesh, P.S., Kim, T.H., Kim, H.D.: Numerical study on shock train characteristic in divergent channels, *Journal of Applied Fluid Mechanics,* Vol. 13, No. 4, pp. 1081-1092, 2020. https://doi.org/10.36884/jafm.13.04.30837

[19] Tolentino, S.L., Mírez, J., Caraballo, S.A.: Numerical analysis of the shock train in conical nozzles with straight-cut throats, *FME Transactions***,** Vol. 52, No. 2, pp. 186-195, 2024. https://doi.org/10.5937/fme2402186T

[20] Tolentino, S. L. and Mírez, J.: Throat length effect on the flow patterns in off-design conical nozzles. *FME Transactions*, Vol. 50, No. 2, pp. 271-282, 2022. https://doi.org/10.5937/fme2201271T

[21] Tolentino, S.L., Mírez, J., Caraballo, S.A.: Numerical analysis of the shock train evolution in planar nozzles with throat length, *FME Transactions*, Vol. 51, No. 4, pp. 595-605, 2023. https://doi.org/10.5937/fme2304595T

[22] Mousavi, S.M., Roohi, E.: Three dimensional investigation of the shock train structure in a convergent-divergent nozzle, *Acta Astronautica,* Vol. 105, No. 1, 2014, pp. 117-127. https://doi.org/10.1016/j.actaastro.2014.09.002

[23] Roy, A., Ghosh, S.: Large-eddy simulation of shock train in convergent-divergent nozzles with isothermal walls, *Journal of Turbulence***,** Vol. 25, No. 9, pp. 318-341, 2024. https://doi.org/10.1080/14685248.2024.2388314

[24] Yuan, T.F., Zhang, P.J., Liao, Z.M., Wan, Z.H.: Effects of inflow Mach numbers on shock train dynamics and turbulence features in a back pressured supersonic channel flow, *Physics of Fluids*, Vol. 36, No. 2, pp. 026126, 2024. https://doi.org/10.1063/5.0187688

[25] Zhang, Z., Cheng, C., Zhang, L.: Asymmetry of oblique shock train and flow control. *Proceedings of the Institution of Mechanical Engineers, Part G: Journal of Aerospace Engineering*, Vol. 238, No. 4, pp. 427-438, 2024. https://doi.org/10.1177/09544100241232160

[26] Li, N.: Response of shock train to fluctuation angle of attack in a scramjet inlet-isolator, *Acta Astronautica*, Vol. 190, No. 8 pp. 430-443, 2022. https://doi.org/10.1016/j.actaastro.2021.10.019

[27] ANSYS-Fluent (2020). Ansys Fluent Theory guide 2020R1.

[28] Menter, F., Egorov, Y.: The Scale-Adaptive Simulation Method for Unsteady Turbulent Flow Predictions. Part 1: Theory and Model Description, *Journal Flow Turbulence and Combustion*, Vol. 85, pp. 113–138, 2010. https://doi.org/10.1007/s10494-010-9265-4

[29] Anderson, J.D: *Fundamentals of aerodynamics*, McGraw-Hill Education: New York, 2017.

[30] Tolentino, S.L.: Experimental and numerical study of the pressure of the water flow in a Venturi tube, *Ingenius*, No. 23, pp. 9-22, 2020. https://doi.org/10.17163/ings.n23.2020.01

[31] Tolentino, S.L., González, O., Mírez, J.: Comparative evaluation of DES and SAS turbulence models for incompressible Flow in a Venturi tube, *INCAS Bulletin,* Volume 14, No. 2, pp. 87-101, 2022. https://doi.org/10.13111/2066-8201.2022.14.2.8

[32] Tolentino, S.L.: Evaluation of turbulence models for the air flow in a transonic diffuser, *Revista Politécnica*, Vol. 45, No. 1, pp. 25-38, 2020. https://doi.org/10.33333/rp.vol45n1.03 (In spanish)

[33] Tolentino, S.L.: Evaluation of turbulence models for air flow in a planar nozzle. *Ingenius*, No. 22, pp. 25-37, 2019. https://doi.org/10.17163/ings.n22.2019.03

[34] Wilcox, D.C.: Reassessment of the scale determining equation for advanced turbulence models, *AIAA Journal*, Vol. 26, No. 11, pp. 1299–1310, 1988, https://doi.org/10.2514/3.10041.

[35] Spalart, P., Deck, S., Shur, M. L., Squires, K. D., Strelets, M. K., Travin, A.: A new version of detached eddy simulation, resistant to ambiguous grid densities. *Theoretical and Computational Fluid Dynamics,* Vol. 20, No. 3, pp. 181–195, 2006. https://doi.org/10.1007/s00162-006-0015-0

[36] Menter, F.R., Kuntz, M., Langtry, R.: *Ten Years of Experience with the SST Turbulence Model*. Proceedings of the 4th International Symposium on Turbulence, Heat and Mass Transfer 4, Begell House Inc., West Redding, 2003. https://www.yumpu.com/en/document/view/16455902/ten-years-of-industrial-experience-with-the-sst-turbulence-model

NOMENCLATURE

A_e	Nozzle-exit area
A_t	Nozzle-throat area
A_e/A_t	Nozzle expansion ratio
L_c	Convergent section length
L_d	Divergent section length
M_d	Design, Mach number for isentropic flow
M	Mach number
P	Static pressure
P_o	Stagnation pressure
P/P_o	Ratio of static and stagnation pressures

T	Static temperature
T_o	Stagnation temperature
x/L_d	Distance/length ratio, nozzle divergent
y^+	y-plus in shear stress value
α	Half-angle of the divergent section
β	Half-angle of the convergent section
NPR	Nozzle pressure ratio
NPR_d	Design, Nozzle pressure ratio

УПОРЕДНА АНАЛИЗА ОБРАЗАЦА ПРОТОКА У ПЛАНАРНИМ И КОНУСНИМ МЛАЗНИЦАМА СА УСКИМ ДИВЕРГЕНТНИМ УГЛОВИМА

Х. Мирес, Х.А. Мендоса, С.А. Карабаљо, С.Л. Толентино

Образац протока у суперсоничним млазницама које се примењују у ваздухопловној области се стално проучава, јер геометријски профили унутрашњих зидова имају значајан утицај на развој режима протока. У овом раду, циљ је да се изврши упоредна анализа образаца протока у планарним и конусним млазницама са веома уским дивергентним угловима, за полуугао α = 1°, 1,21° и 2°. Вискозно поље протока је симулирано у 2Д помоћу кода ANSYS-Fluent R16.2. RANS модел и SAS модел турбуленције су коришћени за услове протока у прелазном стању. За вискозност као функцију температуре, коришћена је једначина Садерлендовог закона. Нумерички резултати поља протока су добијени за NPR опсег од 3,98 до 6,95. У дивергентном стању је представљен низ ударних таласа, који је за конусну млазницу онај са највећим флуктуацијама брзине у фронтовима ударних таласа. За проток на излазу млазнице, за притисак NPR 6,95, конична млазница са α = 1° има просечно повећање брзине Маховог броја од 8,81% у односу на равну млазницу; слично, за α = 1,21° има повећање од 9,73%, а за α = 2° има повећање од 12,88%, респективно.